Evolution of surface morphology during growth and ion erosion of thin films

R. Schlatmann, J. D. Shindler, and J. Verhoeven

Stichting voor Fundamenteel Onderzoek der Materie Institute for Atomic and Molecular Physics,
Kruislaan 407, 1098 SJ Amsterdam, The Netherlands

(Received 1 May 1996)

A model is presented to describe the evolution of thin-film surface morphology during growth and ion erosion. Characteristic in-plane length scales and overall amplitude of the roughness are studied as a function of certain competing roughening and smoothing mechanisms. Particular attention is paid to the deposition method of growth followed by ion erosion of an excess layer thickness. The model is extended to the case of multilayers, to include roughness correlations between different interfaces. Specular and diffuse x-ray-scattering measurements on Mo/Si multilayers are interpreted in terms of the model. Quantitative agreement between the model and the experimental data can be obtained if we assume viscous flow to be the dominant smoothing mechanism during ion erosion of the Si layers. [S0163-1829(96)09539-2]

I. INTRODUCTION

Integrated circuits, optical coatings, magnetic tapes, and a host of other products of modern technology require the capacity to deposit thin films. The usefulness of such coatings depends heavily on the nature of the surface morphology, i.e., on its height variations, or roughness. Clearly, this dependence is even stronger for multilayers, which exist by virtue of a high number of interfaces. It is therefore important to understand and possibly control the development of the surface of a growing film.

Thin films do not form smooth surfaces under all deposition conditions. Therefore, planar film growth is often promoted by introduction of some energy into the growing film, either by substrate heating or by particle beams, usually consisting of energetic ions. In sputter deposition, these ions are a byproduct of the sputtering of primary target material, but in cross-beam sputter deposition and ion-beam-assisted deposition, the ion beam is specifically directed at the growing surface. This is also true for the technique of ion polishing, pioneered by Spiller[1] and by Puik *et al.*[2] for the deposition of x-ray multilayer mirrors. In this technique, deposition of a layer is followed by ion-beam erosion of a certain excess thickness of the layer until the desired final thickness is reached. Thus, the steps involving growth and ion-beam erosion are separated in time. The process has been called ion polishing because, under certain optimum conditions, surface roughness was found to be reduced as a result of the sputtering. In previous work we have measured amplitudes[3] and in-plane length scales[4] of the roughness of ion-eroded Mo/Si multilayer interfaces. Here we present a model to account for the effects of ion erosion on surface roughness and we interpret previous and new results in terms of this model.

Several roughening and smoothing effects have been identified that can occur during deposition or ion erosion of a layer. Roughening mechanisms include shot noise in the arrival or removal rate of particles[5] and geometrical shadowing of the incident particle beam by surface features.[6] Shadowing will be ignored in our calculations, assuming slopes on the surface to be too small for it to occur. The variation in sputter rate with surface curvature[7] is a third roughening effect, specific for ion erosion. Smoothing mechanisms include surface diffusion,[8] evaporation-recondensation (assuming no net mass change), and bulk diffusion.[8] We will not incorporate the latter two mechanisms, for simplicity as well as for lack of experimental observation of their importance. Smoothing by viscous flow of noncrystalline materials[9] was demonstrated as a result of ion bombardment[10,11] on SiO_2. The surface effect of viscous flow is activated by the ion beam, which creates defects in the solid, and driven by the surface tension, which tends to minimize surface curvature.

In our model, we closely follow the derivation and terminology of the growth model of Stearns[12,13] and Spiller, Stearns, and Krumrey,[14] who also generalized the description of surface morphology to the case of multilayers. This means that we assume growth to occur only in the direction perpendicular to the (average) surface. The more general case of growth along the local surface normal was treated by Kardar, Parisi, and Zhang.[15] For relatively smooth surfaces, however, this simplification will be valid. Our inclusion of smoothing and roughening mechanisms differs from that of Stearns and Spiller, but is equivalent to the treatment by Mayer, Chason, and Howard.[16] Thus, roughness is introduced by shot noise in the deposition rate, and by variations in the ion-erosion rate with surface curvature. Smoothing mechanisms in our model are surface diffusion and viscous flow. The latter is only taken into account during ion erosion.

There have been numerous measurements of surface morphologies,[17] using a variety of techniques such as x-ray and electron reflectivity, scanning tunneling microscopy (STM) and atomic force microscopy (AFM), ellipsometry, and electron microscopy. The work most closely related to ours includes a number of x-ray-reflectivity studies on multilayers,[14,18,19] ion-eroded SiO_2,[16,20] and Ge (Ref. 21) surfaces, as well as STM studies of ion-eroded graphite.[22,23,24] Although ion polishing has been used quite successfully to reduce surface roughness,[3,25–28] no specific study has been done to explain the effects observed. Spiller, Stearns, and Krumrey,[14] in the analysis of their data, intentionally averaged over the effects of growth and ion polishing that we want to separate.

In our experiments we have used x-ray scattering, which is one of the techniques that can probe the relevant length scales in the problem of surface roughness. In many areas of

materials research, on solids,[29,30] liquids,[31–33] and liquid crystals,[34] diffuse x-ray scattering has been used to gain insight into the lateral distribution of surface roughnesses. The technique has the advantage that it is nondestructive, that it can probe relatively large sample areas (of the order of a few mm^2), and that all interfaces of a multilayer can be probed simultaneously. The latter property of x-ray scattering makes it sensitive to correlations between roughness at different interfaces, but it also complicates the extraction of detailed information on specific interfaces of a multilayer. Furthermore, the information obtained is in reciprocal space, not real space.

This paper is divided into a theoretical and an experimental part. In Sec. II, we introduce the basic equations to describe surface morphology. Next, we explicitly describe the separate steps of growth and ion erosion, in terms of this model. We study the effect of variation of the excess layer thickness, and the effect of varying the relative strength of roughening and smoothing mechanisms during growth and ion erosion. More specifically, we study the development of characteristic length scales and overall amplitude of the surface roughness. We find predictions for optimum deposition conditions. The extension to the case of multilayers is made, which includes calculation of correlations of the roughness at different multilayer interfaces. The experimental part of this paper, Secs. V–VII, is concerned with diffuse x-ray-scattering measurements, to determine the in-plane size distributions of the roughness of several Mo/Si multilayers, grown with and without ion-beam erosion. The results are interpreted in terms of the model introduced in the theoretical part.

II. BASIC MODEL EQUATIONS

Consider a growing film on a perfectly flat substrate with a surface normal $\hat{z}$. Suppose that particles with a volume Ω arrive at random positions. The surface profile of the film at time t is described by a function $h(x,y,t)$, where h is the surface height at a position (x,y). The surface height is measured with respect to an arbitrary reference plane, also with a surface normal $\hat{z}$. With respect to a fixed frame, the average surface height d (=layer thickness) is given by $d=Rt$, where R is the deposition rate. During ion erosion, R will have a negative value. The surface profile $h(x,y)$ has a spatial frequency spectrum $h(\mathbf{q})$, and the two are connected by Fourier transform. For simplicity, we assume a roughness distribution that is independent of azimuthal angle ψ, so that we can reduce the description to one dimension. Thus $h(\mathbf{q})=h(q)$, where $q=2\pi/r$ and r a distance in an arbitrary direction in the (xy) plane. The surface profile $h(q)$ at a certain time $t+\delta t$ is connected to the profile at time t by the recursion relation

$$h_{d+\delta d}(q) = a(q,\delta d)h_d(q) + \eta(\delta d) + \delta d, \qquad (1)$$

where we have made the time dependence implicit by the transformation $\delta d = R\,\delta t$. The replication factor $a(q,\delta d)$ [$=a(q,R\,\delta t)$] accounts for propagation of surface features through the new layer δd. Any physical model assumptions are contained in the function $a(q,\delta d)$. The term η is a frequency-independent (i.e., ''white'') noise term in the deposition rate, proportional to t. We will choose the plane

of the average surface, at any given time t, as our reference plane. In other words, we measure the height deviations rather than the absolute values, and we remove δd from the right-hand side of Eq. (1).

One can define the power-spectral density (PSD) of the height variations on the surface as $\mathrm{PSD}(q;d) \equiv \langle h_d(q)h_d^*(q)\rangle$, where the brackets denote an average over an ensemble of statistically equivalent surfaces. The Fourier transform of the PSD (with respect to the spatial coordinates), is the height-height correlation function $C(r,d)$ of the surface. Given the basic relation of Eq. (1), and the assumption that the shot noise in the particle arrival rate is described by Poissonian statistics, it was shown by Spiller, Stearns, and Krumrey[14] that the power-spectral density can be expressed as a function of film thickness d and spatial frequency q as

$$\mathrm{PSD}(q;d) = 4\Omega\,\frac{1-\exp[-2b(q)d]}{2\pi b(q)}, \qquad (2)$$

where $b(q)$ is defined by $a(q,d)=\exp[-b(q)d]$.

We must define the function $b(q)$ now by the choice of description of the inclusion of smoothing and roughening mechanisms. Here, we deviate from the description of Spiller, Stearns, and Krumrey. Following the approach used by Mayer, Chason, and Howard, we write

$$b(q) = Vq - Kq^2 + Dq^4. \qquad (3)$$

Smoothing by viscous flow is modeled by the term in $b(q)$ proportional to q.[9] The proportionality constant V is equal to $\gamma/R\eta_v$, where γ is the surface tension and η_v is the coefficient of viscosity. The frequency-dependent roughening effect of sputter-yield variations with surface curvature[7] is included by the term in $b(q)$ proportional to q^2. The proportionality constant K is dependent on the angle of incidence of the ions, θ, and the azimuthal angle ψ. For simplicity we will assume no dependence on ψ, so that we can keep the calculations one dimensional, but following the model of Bradley and Harper,[7] this can easily be changed if necessary. The third term in Eq. (3), proportional to q^4, describes smoothing by surface diffusion.[9] The proportionality constant D is given by

$$D = \frac{D_s\Omega^2\rho_s\gamma}{RkT}, \qquad (4)$$

with D_s the surface diffusion constant, ρ_s the number of atoms per unit surface, k the Boltzmann constant, and T the absolute temperature. During growth, the values of V and K are set to zero. For clarity we will derive results in the rest of this paper by treating the cases of smoothing by surface diffusion and viscous flow separately. There is no a priori reason why they should not occur simultaneously, but the differences between their effects can thus be demonstrated more clearly.

One can also write down an expression for the PSD of a layer grown on a rough substrate:

$$\mathrm{PSD}_{tot}(q,d) = \mathrm{PSD}_{int}(q,d) + a^2(q,d)\mathrm{PSD}_{sub}(q), \qquad (5)$$

where the total $\mathrm{PSD}_{tot}(q,d)$ is composed of a contribution $\mathrm{PSD}_{int}(q,d)$, the intrinsic PSD of the film grown on a perfectly smooth substrate, and $\mathrm{PSD}_{sub}(q)$, the PSD of the substrate. The latter is attenuated by the replication factor squared [$a^2(q,d)$].

Because the PSD is connected by (spatial) Fourier transform to the correlation function $C(r)$, we can write down a straightforward relation between the rms roughness σ_{rms} and the PSD:

$$C(0) = \sigma_{rms}^2 = \frac{1}{4\pi^2} \int_{-\infty}^{\infty} \int_{-\infty}^{\infty} PSD(\mathbf{q}) d^2 q$$

$$= \frac{1}{2\pi} \int_0^{\infty} q PSD(q) dq, \qquad (6)$$

where we have made use of the fact that the roughness is assumed isotropic in the surface plane. It is important to note that any value of σ_{rms}, when found in experiment, is always determined by the resolution of the measurement. The instrument will have some lower and upper frequency limits that must be used in the integration in Eq. (6). For x-ray-scattering measurements, the lower frequency limit q_{min} will be determined by the coherence length of the x-ray beam. In STM and AFM experiments, it will be limited to the frequency corresponding to the maximum scanning range. Physically, the upper limit can never exceed a value of $q_{max} \approx \pi/l$, where $l = \sqrt[3]{\Omega}$, the basic particle (atom) size.

III. GROWTH AND ION EROSION

Now we extend the equations of the preceding section, in order to explicitly account for the temporal separation of growth and ion bombardment in the ion-polishing technique. Unless stated otherwise, we assume that K is very small. We can rewrite Eq. (5) for the PSD of a final layer thickness d as

$$PSD(q,d,\Delta d) = \exp[-2b_i(q)\Delta d]$$

$$\times \Omega \frac{1 - \exp[-2b_g(q)(d+\Delta d)]}{2b_g(q)}$$

$$+ \Omega \frac{1 - \exp[-2b_i(q)\Delta d]}{2b_i(q)}, \qquad (7)$$

where the subscripts g and i denote values during growth and ion erosion, respectively. The first term on the right-hand side of the equation describes how the roughness, resulting from growth of a layer of thickness $d+\Delta d$, is attenuated [through $a(V,K,D_i,\Delta d)$] by ion erosion of the excess layer Δd. The second term describes the intrinsic roughness that results from the ion erosion of a layer of thickness Δd. Thus, the layer after growth is treated as the substrate for the subsequent ion-bombarded layer of thickness Δd. The PSD of a layer of given thickness d now depends on the excess layer thickness Δd and on the value of $b_i(q)$ with respect to $b_g(q)$. In order to be useful, the smoothing during ion erosion must outweigh the (inevitable) roughening during growth and ion erosion of a layer of thickness Δd.

Using Eq. (7), we calculate a number of typical trends in the PSD upon variation of its parameters. We start with the development of the PSD as a function of Δd. In the calculation d and Ω can be fixed at arbitrary values (they will simply scale the results). We plot the results in Fig. 1.

The two main characteristics that we observe are a reduction in the PSD at large frequency (and an increase at low frequency), and an increase of the characteristic length ξ of the PSD with increasing Δd. This a typical result as long as
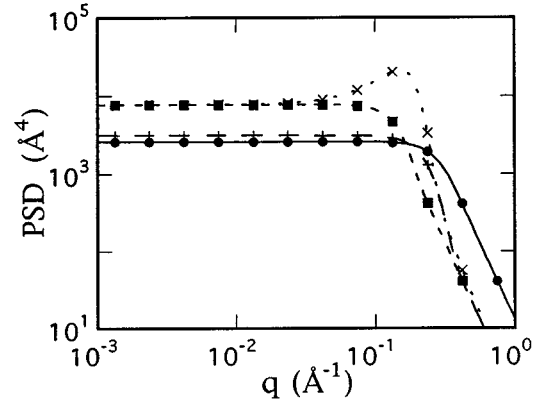
FIG. 1. Double-logarithmic plot of the power-spectral density function PSD vs spatial frequency $\mathbf{q}$ for different values of Δd. Fixed parameters are $D_g = 1$ Å^3 and $D_i = 10$ Å^3, $\Omega = 27$ Å^3, $d = 100$ Å, $V = 0$, and $K = 0.01$ Å. (a) $\Delta d = 0$ (●), (b) $\Delta d = 10$ Å (+), (c) $\Delta d = 100$ Å (■), (d) $\Delta d = 100$ Å, $K = 0.5$ Å (×).

the ratio D_i/D_g is chosen larger than unity and the effect of K is small. Asymptotically, the value of ξ will be determined by growth or ion-erosion parameters only: $\xi(\Delta d \to 0) = 2\pi\sqrt[4]{2D_g d}$ and $\xi(\Delta d \to \infty) \approx 2\pi\sqrt[4]{2D_i \Delta d}$ or $\xi(\Delta d \to \infty) \approx 4\pi V \Delta d$. In other words, for a very small excess layer, the ion erosion will hardly have changed the surface, whereas for very large Δd, the layer will have "forgotten" its state before the ion bombardment. We have also plotted the result for one very large value of K. In that case, a characteristic, dominating frequency, is seen in the power spectrum of the roughness.

As a result of the different q dependence of $b(q)$ on V and D, there is an important difference in the shape of the resulting PSD, depending on the dominant smoothing mechanism. We consider two layers with the same rms roughness. In the one case, the layer was smoothed by viscous flow only, and the other case by surface diffusion only. In Fig. 2 we plot the power spectrum for both cases. We see that the result of viscous flow with respect to surface diffusion is a larger characteristic length ζ and a slower power-law falloff at large q, with a power of 1 instead of 4.

Next, we calculate the rms roughness σ_{rms} as a function of Δd. Thus, we explore the magnitude and limits of the smoothing effect of ion erosion. We will do so for the case of smoothing by surface diffusion, but the same qualitative results can also be found for smoothing by viscous flow. In the calculation, we use $q_{max} = 1$ Å^{-1} and $q_{min} = 10^{-5}$ Å^{-1}, which are realistic values for the upper and lower frequency cutoffs. The results for different ratios of D_i/D_g are plotted in Fig. 3. As expected, we see no smoothing if D_i/D_g is smaller than or even equal to unity and increased smoothing with increasing D_i/D_g, for values larger than unity. We see that for each value of $D_i/D_g > 1$ there is a certain optimum excess layer thickness Δd_{opt}, a result that had already been found in experiment[2] and that can be derived analytically as well.[35] For larger K, the same result is found, qualitatively, except that the minimum of σ_{rms}, as a function of Δd, is less deep and more pronounced. For every large K, there will be no smoothing effect left.
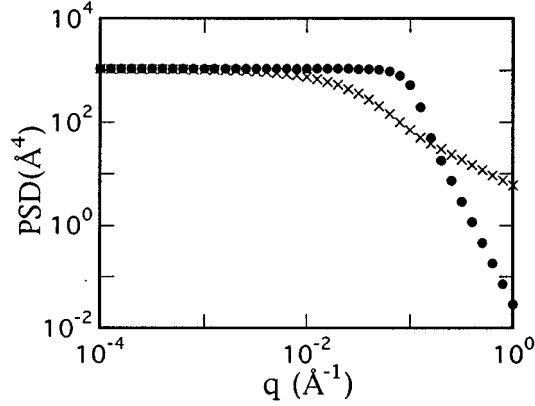
FIG. 2. Double-logarithmic plot of PSD(q), with $\sigma=1$ Å for both calculations. The different curves represent the two extreme cases of (a) smoothing caused by surface diffusion ($\bullet$), and (b) smoothing caused by viscous flow ($\times$).

IV. MULTILAYERS

We extend the calculations to the case of multilayers. The PSD of the first layer is found by applying Eq. (7) and is subsequently used as the substrate PSD in Eq. (5). This way, we can calculate the PSD, σ_{rms}, and Δd_{opt} for each of the layers.

One can also calculate the power spectrum of correlations in the roughness of different interfaces. As was shown by Stearns,[12] we can define the PSD of roughness correlations between interfaces i and j (with $i \geq j$) as

$$\mathrm{PSD}_{i,j}(q) = \langle h_i(q) h_j^*(q) \rangle = \sum_{n=0}^{j} c_{in} c_{jn} \mathrm{PSD}_{\mathrm{int},n},$$

$$\text{with } c_{kn} = \prod_{l=n+1}^{k} a_l(q,d), \qquad (8)$$

where the intrinsic roughness of interface n, as given in $\mathrm{PSD}_{\mathrm{int},n}$ is assumed to be uncorrelated with the *intrinsic* roughness of interface k, for $k \neq n$. Thus, the correlations are
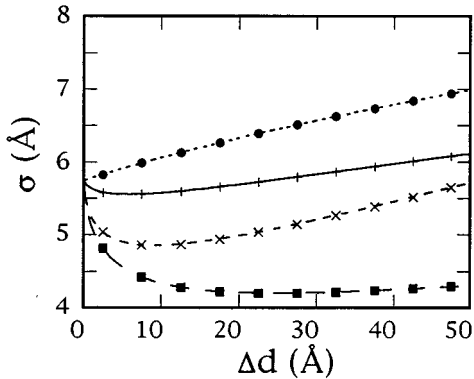
FIG. 3. Roughness as a function of the excess layer thickness Δd, for a number of values of D_i/D_g. Fixed parameters are $V=0$, $K=0.01$ Å, $d=100$ Å, and $\Omega=27$ Å^3. The different curves represent (a) $D_g=D_i=1$ Å^3 ($\bullet$), (b) $D_g=1$ Å^3, $D_i=2$ Å^3 (+), (c) $D_g=1$ Å^3, $D_i=10$ Å^3 ($\blacksquare$), and (d) $D_g=1$ Å^3, $D_i=10$ Å^3, and $K=0.35$ Å ($\times$).
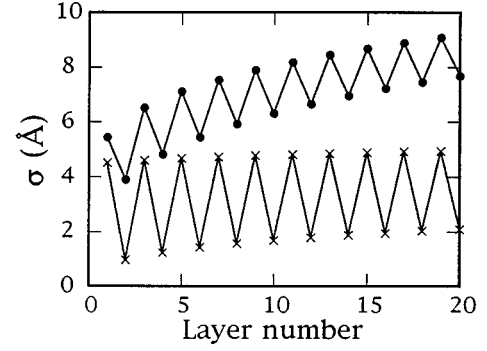
FIG. 4. Development of the rms roughness σ_{rms} of a Mo/Si multilayer as a function of layer number. Fixed calculation parameters are $d_{\mathrm{Mo}}=25$ Å, $d_{\mathrm{Si}}=35$ Å, $\Omega_{\mathrm{Mo}}=20.4$ Å^3, $\Omega_{\mathrm{Si}}=13.0$ Å^3, $D_{g,\mathrm{Mo}}=0.1$ Å^3, $D_{i,\mathrm{Mo}}=2$ Å^3, $K_{\mathrm{Mo}}=0.16$ Å, $D_{g,\mathrm{Si}}=0.9$ Å^3, $D_{i,\mathrm{Si}}=1500$ Å^3, and $K_{\mathrm{Si}}=0$ Å. Plotted are (a) no ion bombardment: $\Delta d_{\mathrm{Mo}}=\Delta d_{\mathrm{Si}}=0$ ($\bullet$); (b) ion bombardment of Mo and Si layers: $\Delta d_{\mathrm{Mo}}=\Delta d_{\mathrm{Si}}=15$ Å ($\times$). The lines are to guide the eye. Results almost equal to those for case (b) are found when $D_{i,\mathrm{Si}}=0$ and $V_{\mathrm{Si}}=1.0$.

found by adding the propagated contributions from all interfaces up to j, being the lower one of i and j. One can also define a function $\mathcal{P}(q)$ as the sum of correlations from all N interfaces:

$$\mathcal{P}(q) = \sum_{i=0}^{N} \sum_{j=0}^{N} \mathrm{PSD}_{i,j}(q). \qquad (9)$$

In Sec. V D, it will be shown that under certain conditions $\mathcal{P}(q)$ is proportional to the diffusely scattered x-ray intensity $I(q_r)$ for $q=q_r$. Here, q_r is the component of the scattering vector parallel to the surface.

In Fig. 4, we show the development of the rms roughness of a Mo/Si multilayer as a function of layer number. We make use of model parameters that we extracted from fits to experimental data (rms roughness values only) in previous work.[3,35] For the ion-eroded multilayer, the smoothing effect is almost entirely due to the ion erosion of Si. Therefore, the Mo-on-Si interfaces have a lower roughness than the Si-on-Mo interfaces, but either type of interface is seen to have a rather constant roughness from substrate to surface. The roughness of the interfaces of the multilayer that was not ion eroded is seen to increase steadily with increasing layer number.

From fits to rms roughness values alone, no conclusions can be drawn as to the dominant smoothing mechanism during ion erosion. But, when we compare the two extreme cases of smoothing caused by surface diffusion only, and smoothing caused by viscous flow only, we see a large difference in the shape of $\mathcal{P}(q)$. In Fig. 5, we plot $\mathcal{P}(q)$ as a function of q. Clearly, the effect of viscous flow is seen at much smaller q than that of surface diffusion, as we saw before in Fig. 2. More importantly, plotted on a log-linear scale, $\mathcal{P}(q)$ is virtually a straight line (proportional to $-q$) for the case of smoothing by viscous flow, whereas surface diffusion will yield a line shape proportional to $-q^4$.
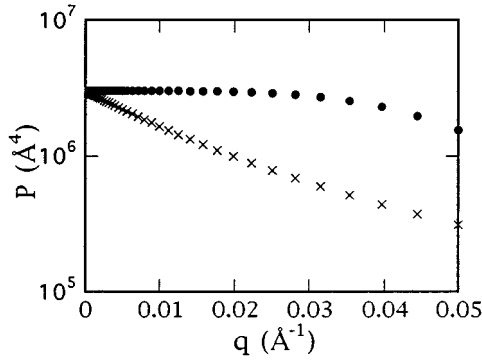
FIG. 5. Calculation of $\mathcal{P}(q)$ using the same parameters as in Fig. 4(b). The different curves represent the two extreme cases of (a) smoothing caused by surface diffusion (●), setting $D_{i,Si}$ $= 1500$ Å^3 and $V_{Si}=0$, and (b) smoothing caused by viscous flow (×), setting $D_{i,Si}=0$ and $V_{Si}=1.0$.

V. EXPERIMENT

A. Sample deposition

The multilayers were deposited on 10×25-mm substrates, cut from Si(111) wafers from which we did not remove the native oxide layers. We used an UHV (base pressure 10^{-7} Pa) electron-beam evaporation system.[36] All layers were deposited at a rate of 0.1 Å/s. The as-grown reference multilayer will be called sample A. For ion-beam erosion, we used a Kaufman source with a 3-cm beam diameter. The 300-eV Kr$^+$ ions were incident at an angle of 45° with the surface normal, with a flux of 10^{14} ions/cm^2 s. The excess layer thickness removed from each of the layers after deposition was different for the three ion-eroded samples. The values we used were 5 Å (sample B), 15 Å (sample C), and 30 Å (sample D), corresponding to a fluence of 0.4, 1.2, and 2.4×10^{16} ions/cm^2 per layer, respectively. The layer thicknesses during deposition and ion erosion were controlled by *in situ* soft-x-ray reflectivity. For these multilayers the soft x-ray line used was C-$K\alpha$, with a wavelength $\lambda=44.7$ Å. Given the grazing angle of incidence of 25° and the optical constants of the materials deposited, the Bragg relation gives an interference period in the measured reflectivity signal of about 60 Å. Each of the multilayers used in the x-ray-scattering experiments consisted of ten periods of Mo and Si layers covered with a 60-Å Si layer to exclude atmospheric influences on the actual multilayer itself.

B. X-ray-scattering setup

The x-ray generator is an Enraf-Nonius GX-21, operated at 8 kW maximum power. In the scattering configuration described below, we obtain a primary beam of 8.4×10^8 photons/incident on the sample. The samples were enclosed in an evacuated cell to reduce nonsample background scattering to near-dark-count levels of ≈0.05 c/s. This allowed a dynamic range of nearly ten orders of magnitude in the measured intensity, enabling us to probe very small in-plane length scales.

Details of the scattering configuration are described elsewhere.[37] In brief, it employs a bent graphite monochromator that focuses the beam in the out-of-plane direction onto the sample. Although both Cu-$K\alpha_1$ and Cu-$K\alpha_2$ lines are selected with this monochromator, the moderate resolution obtained is dominated by the angular beam divergence. The incident in-plane beam divergence, $\Delta\alpha$, is defined by a slit set between the monochromator and the sample, while slits immediately before a scintillation detector define the in-plane detector acceptance, $\Delta\beta$. Out of the scattering plane, all slits are left wide open. Thus, we effectively integrate the intensity in this direction. For this work, $\Delta\alpha=\Delta\beta=0.08°$ full width at half maximum (FWHM). Such symmetric resolution is advantageous for diffuse scattering measurements, as opposed to the usual case where the emphasis is on the measurement of the specular signal and typically $\Delta\alpha\ll\Delta\beta$. In this paper, fitted models include a convolution with resolution.

The beam size, in the plane perpendicular to the propagation direction, was approximately 0.2×3 mm^2 at the sample; the samples themselves were 25×10 mm^2. Thus, overfilling of the sample occurred for incident angles $\alpha\lesssim0.5°$. In addition, when the detector angle $\beta\gg\alpha$ and α small, the signal may also be reduced if the beam footprint on the sample is larger than the sample area visible by the detector. This latter effect is one possible cause of asymmetry in transverse sample rocking scans. Both of these geometric effects have been corrected for in the data shown.

C. X-ray-scattering geometry

In the experiments described, we have taken three types of scans: Specular reflectivity scans, in which the grazing angle of incidence α of the x rays is equal to the outgoing angle β; off-specular scans, where the sample is offset from the specular condition by a small angle ω such that $\omega=(\beta-\alpha)/2$; and transverse scans, where ω is varied, but the total scattering angle $\alpha+\beta$ is kept fixed. If the wave vector $\mathbf{k}$, with $|\mathbf{k}|=2\pi/\lambda$, and the wave vector transfer $\mathbf{q}=\mathbf{k}_{out}-\mathbf{k}_{in}$ are defined, one can derive the reciprocal-space equivalent of these scans. Specular scans probe only in the direction perpendicular to the interfaces. The spatial coordinates are chosen such that the surface normal is along $\hat{z}$, and thus specular scans probe reciprocal space along q_z. From these scans we extract the spacing of the interfaces and the total interfacial widths. Off-specular scans probe in both q_z and q_r (in-plane) directions, and are used to measure the degree of conformality of roughness at different interfaces. Transverse scans probe along the q_r, i.e., the in-plane direction for $\alpha+\beta$ small, with $q_r=q_z\tan\omega$. They yield the information of most interest to this experiment. At $\alpha=0$ and $\beta=0$, the sample will block the ingoing and outgoing x-ray beams, respectively. This determines the maximum scan range in a transverse scan, where $\alpha+\beta$ is constant, to $q_r=\pm q_z\tan[(\alpha+\beta)/2]$ (note that this restriction does not apply when the detector arm can be moved out of the reflection plane, such as in standard surface diffraction experiments[38]). In the next section, we show how transverse scans are connected to the interfacial correlation function that we are interested in.

All x-ray scattering measurements shown have been normalized to the incident beam intensity. The true specular signal has been obtained by subtracting the off-specular scan (offset angle $\omega=0.15°$) from the raw specular signal. In this way, the diffuse contribution at $q_r=0$ is almost completely removed. Figure 6 shows specular and off-specular scans for the four samples with different ion-eroded thicknesses Δd.

All transverse scans shown have been footprint and background corrected, and have also been corrected for the changing illuminated area on the sample during the scan ($1/\sin\alpha$ correction). Background levels were calculated from points at which $\alpha \lesssim 0$ or $\beta \lesssim 0$. Data around several integer Bragg orders are shown in Fig. 7. We also measured two transverse scans from sample D (with the largest ion-bombarded-excess layers), to check whether there is any anisotropy visible in the surface morphology. The scans were taken with the ion-beam direction in, and perpendicular to the scattering plane, but no measurable difference could be found between the two scans. Hence, we conclude that we can treat the ion-beam erosion as isotropic in the surface plane.

D. X-ray-scattering theory

To analyze our data, we split the calculated intensity into a specular and a diffuse part. To fit the specular signal, we use the recursive dynamical method of Parrat.[39] The analysis of the diffuse part of the x-ray scattering is based on the formalism developed by Sinha *et al.*[29] They have shown that in the first Born approximation for a single surface, the scattering cross section per unit area surface is given by

$$S(\mathbf{q}) = (r_e \Delta \rho)^2 \, e^{\dfrac{-q_z^2 \sigma_t^2}{q_z^2}} \int \int_{S_0}$$

$$\times dX \, dY \, e^{q_z^2 C(X,Y)} e^{-i(q_x X + q_y Y)}, \quad (10)$$

where the integral is over the coherence area of the beam on the sample. The term $\Delta\rho$ gives the change in electron density at the interface, and r_e is the classical electron radius. A height-height correlation function, the Fourier transform of $PSD(\mathbf{q})$, has been defined as $C(X,Y) = \langle h(X,Y)h(0,0)\rangle$, the brackets denoting a statistical average over the whole surface, where $C(0,0) = \sigma_r^2$. The total interfacial width is given by $\sigma_t^2 = \sigma_r^2 + \sigma_m^2$, where σ_r and σ_m denote roughness and intermixing contributions, respectively. The intermixing can be assumed to be uncorrelated, or zero-length-scale roughness. It will not cause backward-diffuse scattering, but it will lower the specular intensity, which is sensitive to the total interfacial width. Corrected for geometric factors such as beam width, sample area, and slit sizes, and convolved with the resolution function at fixed q_z, $S(\mathbf{q})$ is proportional to the measured intensity as a function of q_r.

We extend the derivation to the case of scattering from multilayers and account for refraction and absorption by calculating the complex scattering vectors inside the multilayers. Then, if one also explicitly integrates over one in-plane direction of $\mathbf{q}$, to account for the fact that the detector slit is wide open in that direction,[29] one can find for the diffuse part of $S(\mathbf{q})$

$$S_{\text{diff}}(q_r) = \sum_{i=1}^{N} \sum_{j=1}^{N} r_e^2 \Delta\rho_i \Delta\rho_j \, \frac{e^{-iq_z d_{ij}} e^{-q_z^2(\sigma_{t,i}^2 + \sigma_{t,j}^2)/2}}{q_z^2}$$

$$\times \int_{-\infty}^{\infty} dr (e^{q_z^2 C_{i,j}(r)} - 1) e^{-iq_r r}, \quad (11)$$

where the double sum runs over all N interfaces, each with a certain width σ_t. The term d_{ij} denotes the distance between the average position of the interfaces i and j. Note that the
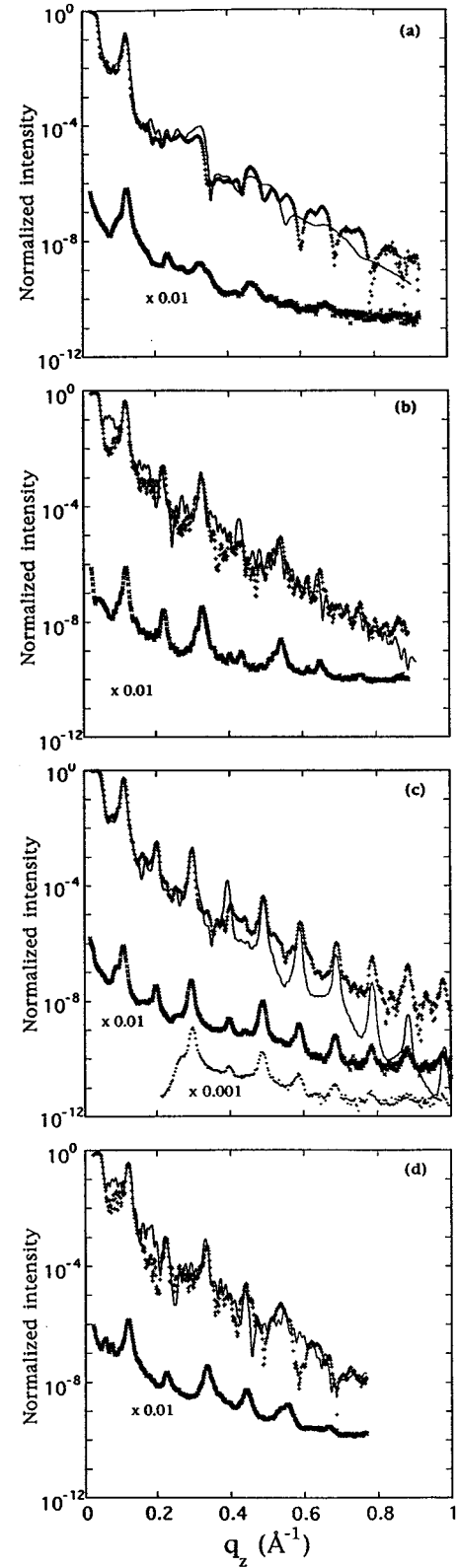
FIG. 6. Specular intensity ($+$) and off-specular ($\times$) intensity at offset angle $\omega = 0.15°$. Symbols represent measured intensities, solid lines represent fits. For clarity, off-specular scans have been shifted downward by an amount indicated in the figure. (a) Sample A, no ion erosion. (b) Sample B, ion-eroded excess layer thickness $\Delta d = 5$ Å. (c) Sample C, $\Delta d = 15$ Å; also plotted is an off-specular scan at offset angle $\omega = 1.5°$ (●). (d) Sample D, $\Delta d = 30$ Å.
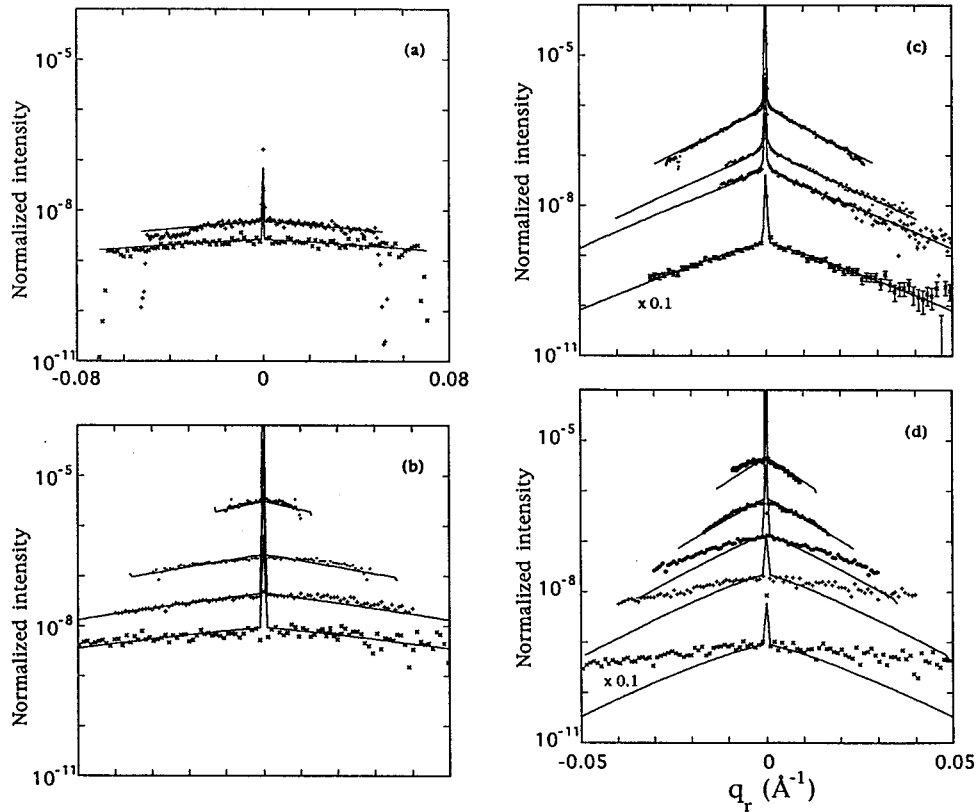
FIG. 7. Transverse-scan intensities at a several values of q_z, corresponding to higher-order Bragg peaks, visible in Fig. 6. For clarity, some curves have been shifted and points beyond the critical angle have been removed for the ion-eroded samples. Symbols represent measured intensities, solid lines represent calculations using the model explained in the text. (a) As-deposited sample at $q_z=0.66$ Å^{-1} (+) and $q_z=0.76$ Å^{-1} (×). The sharp drop in intensity at the critical angle shows that the data are far above background. (b) Sample B, $\Delta d=5$ Å at $q_z=0.33$ (■), 0.54 (●), 0.65 (+), and 0.76 (×) Å^{-1}. (c) Sample C, $\Delta d=15$ Å at $q_z=0.49$ (■), 0.59 (●), 0.69 (+), and 0.79 (×) Å^{-1}. (d) Sample D, $\Delta d=30$ Å at $q_z=0.33$ (■), 0.44 (△) 0.54 (●), 0.63 (+), and 0.72 (×) Å^{-1}.

specular part of the scattering has been explicitly subtracted out. The correlation function $C(r)$, assuming roughness that is isotropic in the plane of the interface, now has been defined to include correlations of the heights in one interface, or between different interfaces: $C_{i,j}(r)=\langle u_i(r)u_j(0)\rangle$. It represents the Fourier transform of PSD$_{i,j}(q_r)$, which was defined in Sec. IV. If such cross correlations exist, i.e., if $C_{i,j}(r)$ is nonzero for $i\neq j$, then the exponential term with $q_z d_{ij}$ as the phase gives the interference between diffusely scattered amplitudes. Such interference gives rise to "quasi-Bragg" peaks in the diffuse intensity,[18] measured as a function of q_z.

For $q_z\sigma_r\ll1$, we expand the exponential function in the integrand of Eq. (11), using only the first two terms. Then, it can be seen that $S_{\text{diff}}(\mathbf{q})$ is directly proportional to the power-spectral density.[29] However, at Bragg angles close to the critical angle for total reflection, i.e., for small q_z, these multilayers are very strong scatterers for which the Born approximation breaks down. This means that for the analysis of transverse scans at low q_z, a dynamical theory, i.e., including multiple scattering, is needed. This type of theory was also developed by Sinha et al. for a single interface and extended to the case of multilayers in a significant number of recent papers, among others by Holy et al.[40] This type of theory essentially involves a calculation of the total electric field at each of the interfaces, with those values as prefactors

to the integral in Eq. (11). When the incident or exit angles equal a lower-order Bragg angle, the electric fields of incoming and outgoing waves have similar amplitudes and add in phase, and the total electric field, and thus the diffuse intensity, is enhanced. For multilayers, one can then observe peaks[18,41] in the diffusely scattered intensity. It may be important to note that these peaks, resulting from an enhanced electric field, show up *as a function of q_r*. They are not the same as the peaks that result from the correlations in roughness between different interfaces, mentioned in the preceding paragraph, which show up *as a function of q_z*. Nonetheless, in transverse scans at large q_z the dynamical peaks are weak, and we can analyze these scans using Eq. (11).

VI. RESULTS AND ANALYSIS

A. As-deposited sample

The specular measurement from the reference (as-deposited) multilayer is plotted in Fig. 6(a). In previous work,[3,35] we gave a detailed study and discussion of the development of σ_t as a function of layer thickness. There we found that our best fit to the peaks in the specular measurement was achieved using an interfacial width ranging from 3 Å at the substrate up to 9 Å at the top surface (see Fig. 4, where the given growth diffusivity model parameters corre-

TABLE I. Experimentally determined and model values of the rms roughness σ and characteristic length ξ_0 for the different samples. All numbers are in Å.

	Experimental values						
Sample	Δd	$\sigma_{t,\mathrm{Mo}}$	$\sigma_{t,\mathrm{Si}}$	$\bar{\sigma}_r$	$\sigma_{m,\mathrm{Mo}}$	$\sigma_{m,\mathrm{Si}}$	ξ_0
A	0	$3\rightarrow9$					
B	5	4.4	3.8	2.3	0.0	3.3	44
C	15	5.1	4.0	1.7	2.2	3.8	107
D	30	5.4	4.3	2.6	2.1	4.2	135
	Model values						
	Δd	$\sigma_{r,\mathrm{Mo}}$	$\sigma_{r,\mathrm{Si}}$	$\bar{\sigma}_r$			ξ_0
B	5	4.4	1.8	3.1			46
C	15	4.6	1.2	2.9			109
D	30	5.1	1.1	3.1			150

spond to surface-diffusion constants of $10^{-21\pm1}$ and $10^{-19\pm1}$ cm^2/s for Mo and Si, respectively.)

In the off-specular measurement at $\omega=0.15°$, a weak reproduction of all peaks in the specular scan can be seen. This indicates some degree of conformality, as we saw in Sec. V D. Furthermore, the transverse scans taken at peaks up to $q_z=0.76$ Å^{-1} (corresponding to a scattering angle $\alpha+\beta=10.32°$) are virtually constant, whereas a loss of conformality at shorter length scales would show up as a decaying intensity at larger q_r values in these scans. From this, we conclude that conformality, i.e., the off-diagonal elements of the correlation function $\mathrm{PSD}_{i,j}(q_r)$, must be constant down to at least the maximum in-plane lengths probed in those scans: 60 Å.

The transverse scans at high q_z values all show an almost constant intensity versus q_r [Fig. 7(a)]. From this, we only conclude that any model for the interfacial correlation function that can give a cutoff in reciprocal space, such as that formulated in a general scaling theory of Kardar et al.,[15] could reproduce this measurement, as long as the model parameters are chosen such that cutoff lies beyond our measured q_r range. The maximum q_r value that we probed corresponds to a cutoff length of 60 Å. Again, we use the mobility parameters D of Mo and Si during growth, found in[35] for this sample. Then, we do indeed find a constant PSD for all q_r values probed. Remarkably, we do not see any influence of the substrate roughness, which might have shown up as a power-law contribution at small q_r.[33] Apparently, the rms roughness is so small that its influence cannot be seen in these measurements. We do not probe at very small q_r because we sacrificed high resolution for a larger dynamic range.

B. Ion-eroded samples

The specular measurements from the ion-eroded samples indicate that the interfacial width is smaller than that of the as-deposited sample. The parameters σ_t that we found for the Si-on-Mo and Mo-on-Si interfaces, by fitting to the peaks in the measured specular signal, are listed in Table I as $\sigma_{t,\mathrm{Mo}}$ and $\sigma_{t,\mathrm{Si}}$, respectively. One can see more higher-order Bragg peaks for sample C than for samples B and D. In this case, that is a result of smaller layer-thickness errors rather than of differences in rms roughness. This also causes the fits to the specular signal to be quite poor overall, because for a good fit to all details we have to find the exact position of each of the interfaces of the multilayer. Nonetheless, this will have no significant effect on the q_r dependence of the calculation of transverse scans.

The off-specular scans (Fig. 6), taken at offset angles of $0.15°$ (and also $1.5°$ for sample C), for all ion-eroded samples show a clear reproduction of the interference peaks that are visible in the specular scan. This means[18,42] that there is some degree of conformality of the roughness between all interfaces, down to in-plane length scales of less than 200 Å.

The transverse scans at high q_z from these samples [Figs. 7(b), 7(c), and 7(d)] show a q_r dependence different from the as-deposited sample. Qualitatively, one can see that the shorter-length-scale (large q_r) roughness is removed more strongly than the long-length-scale roughness.

A striking feature of all transverse scans from these three samples is the exponential decay with q_r of the intensity (observed before for sample C only[4]), which is proportional to $S_{\mathrm{diff}}(q_r)$ in Eq. (11). As we saw in Fig. 5, this is a fingerprint of the dominance of viscous flow as the smoothing mechanism during ion bombardment. It can also be seen that the slope of the exponential decreases for scans taken at larger values of q_z. This is a result of the fact that $S_{\mathrm{diff}}(q_r)$ is not proportional to the PSD, as seen in Eq. (11). In Fig. 8 we plot the measured values of the characteristic length ξ of the exponential decay as a function of q_z. To make a fit to the reflectivity data, we should perform a normal and inverse Fourier transform for every value of i, j, and q_r. Therefore, we derive a simple analytical approximation to the dependence of the line shape on the value of q_z so that we can extrapolate our measured values to $q_z=0$, and simply use the PSD without any Fourier transform.

We start with the assumption that we only look at transverse scans at Bragg peaks, and that $(\sigma_{t,i}^2+\sigma_{t,j}^2)/2$ is the same for all i and j. Then the prefactor to the integral in Eq. (11) is a constant that can be taken out of the double sum. We will further assume that the correlation function for all i and j can be written as a function independent of i and j. Then, given the fact that the Fourier transform of a Lorent-
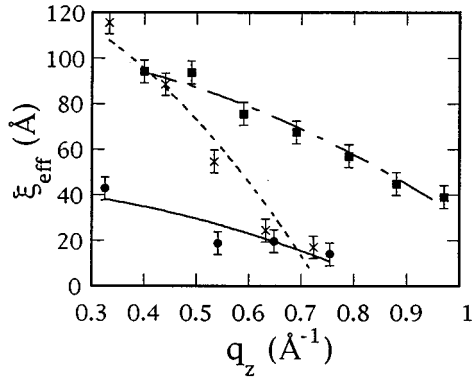
FIG. 8. Measured and calculated values in transverse scans of the effective characteristic length (see text) as a function of q_z, for ion-eroded samples. Fits were performed using the analytical approximation given in the text [Eq. (15)], and the fit parameters listed in Table I. Symbols represent the measured values, lines represent fits. (a) Sample B, $\Delta d = 5$ Å ($\bullet$, full line), (b) Sample C, $\Delta d = 15$ Å ($\blacksquare$, dash-dotted line), (c) Sample D, $\Delta d = 30$ Å ($\times$, dashed line).

zian yields an exponential function, our simplest choice is the following correlation function:

$$C(r) = \frac{\overline{\sigma}_r^2}{1 + (r/\xi)^2},\tag{12}$$

where $\overline{\sigma}_r$ is the average value of $\sigma_{r,i}$ over all interfaces. Because the double sum of Eq. (11) contains $N^2/4$ terms proportional to $\sigma_{r,\mathrm{Mo}}^2$, $N^2/4$ terms proportional to $\sigma_{r,\mathrm{Si}}^2$, and $N^2/2$ terms proportional to $\sigma_{r,\mathrm{Mo}}\sigma_{r,\mathrm{Si}}$, the average value $\overline{\sigma}_r$ is simply found by $\overline{\sigma}_r = (\sigma_{r,\mathrm{Mo}} + \sigma_{r,\mathrm{Si}})/2$.

Although we cannot calculate the Fourier integral in Eq. (11) analytically with the correlation function of Eq. (12), we can make a finite-order expansion of the exponential in the integral, and then integrate each term analytically. We expand in $(q_z\overline{\sigma}_r)^2$, and obtain

$$S_{\mathrm{diff}}(\mathbf{q}) \propto \mathcal{F}(\mathbf{q}) = \pi\xi q_z^2 \overline{\sigma}_r^2 e^{-\xi q_r} \sum_{k=0}^{n} \frac{(q_z^2\overline{\sigma}_r^2)^k}{k!} \sum_{l=0}^{k} a_{kl}(\xi q_r)^l,\tag{13}$$

where $a_{00}=1$, $a_{10}=1/4$, $a_{11}=1/4$, etc. For $q_z\overline{\sigma}_r \ll 1$, we need only the $n=0$ term, and find an exponential line shape of $S_{\mathrm{diff}}(q_r)$, with an exponent that is a constant, independent of q_z. However, when $q_z\overline{\sigma}_r$ increases towards unity, as is the case for much of our data, this first-order approximation breaks down.

If we also include the next order in $(q_z\overline{\sigma}_r)^2$, then $S_{\mathrm{diff}}(q_r)$ can be approximated by

$$S(\mathbf{q_r}) \propto e^{-\xi_{\mathrm{eff}} q_r},\tag{14}$$

where we defined

$$\xi_{\mathrm{eff}} = \xi_0[1 - \tfrac{1}{4}(q_z\overline{\sigma}_r)^2].\tag{15}$$

A fit through the measured exponents as a function of q_z yields a value for ξ_0 and $\overline{\sigma}_r$. These fits are shown in Fig. 8, and the fit parameters are listed in Table I.

Now we can compare these values to the results of the growth model. Assuming that the full smoothing effect of ion-beam bombardment is caused by viscous flow, we should use the value $V_{\mathrm{Si}} = 1 \pm 0.2$, as found previously.[35] The best fit

to the most sensitive observable, ξ_0, is found for a value of $V_{\mathrm{Si}} = 1.2$, for all three samples. In Table I we list all model values, calculated with only that value of V, and the appropriate atomic sizes and layer and excess layer thicknesses. Thus, using $V = \gamma/R\,\eta_v$, and inserting the erosion rate R and a surface tension $\gamma = 1$ J/m^2, we find a viscosity value $\eta_v = 1 \pm 0.2 \times 10^{11}$ Ns/m^2 (for 300 eV Kr). This is of the same order as the (1-keV Xe$^+$)-ion-induced viscosity of Ge, reported recently by Chason et al.[21]

Because we determine σ_t from the specular measurement, and σ_r through the decay of the exponent ξ_{eff} as a function of q_z, we can now separate the contributions σ_r and σ_m, using $\sigma_t^2 = \sigma_r^2 + \sigma_m^2$. The values of σ_m that we derive using the fit parameters $\sigma_{r,\mathrm{Mo}}$ and $\sigma_{r,\mathrm{Si}}$, are also listed in Table I. We find that the intermixing width is much larger for the interfaces of Mo-on-Si than for Si-on-Mo, which is consistent with other authors' findings.[43,44] As an aside, we remark that this extraction of physical information from the q_z dependence of $S_{\mathrm{diff}}(\mathbf{q})$ in transverse scans is completely analogous to the case of scattering from capillary waves on simple liquid surfaces.[32] There, $S_{\mathrm{diff}}(q_r)$ decays as a power law, with an effective power 2η, where η depends on q_z^2 as well as on the surface tension.

We also calculated $S_{\mathrm{diff}}(q_r)$ numerically, using Eq. (11) and the correlation function of Eq. (12). This way, we can check the validity of the values of σ_r and ξ_0 that we obtained from the analytical approximation. As the fits in Fig. 7 show, we do indeed find a good fit to the measured intensities for samples B and C, but deviations for the scans at larger q_z values of sample D. Because this sample has the largest roughness σ_r and the largest loss of correlations from one interface to the next, we assume that in this case our simple approximation starts to break down.

VII. CONCLUSIONS

We have presented a model for the description of surface morphology of thin films. Mathematically, we have followed the derivation of Stearns and Spiller, but we have deviated from their model when including the roughening and smoothing mechanisms that operate during deposition of the film. These were included following Mayer and co-workers.[16]

We have modified the model to account explicitly for the development of surface morphology during growth and subsequent ion bombardment. Physically, the description roughening mechanisms is in terms of shot noise in the deposition or erosion rate, and slope dependence in the erosion rate. Smoothing is assumed to be caused by viscous flow and surface diffusion. Within this model, we have found reproduction of earlier experimental observations such as smoothing ("ion polishing") and an optimum in the excess layer thickness. We have also found predictions for the development of rms roughness, characteristic in-plane lengths, and correlations between multilayer interfaces.

We have measured the diffuse x-ray-scattering intensity from four Mo/Si multilayers, three of which had their interfaces ion eroded, the other not. We have found that the main qualitative difference in interface morphology between ion-eroded and as-grown surfaces, apart from the reduced rms roughness that we found in earlier work, is an increased

characteristic length ξ_0 with increasing ion-eroded layer thickness Δd. From the dependence of diffusely scattered intensity on q_r, we conclude that the ion-beam-induced smoothing must be a result of viscous flow. Using one viscosity parameter, we have been able to reach agreement between measurements and calculations.

[1] E. Spiller, Appl. Phys. Lett. **54**, 2293 (1989).

[2] E. J. Puik, M. J. van der Wiel, J. Verhoeven, and H. Zeijlemaker, Thin Solid Films **193/194**, 782 (1990).

[3] R. Schlatmann, C. Lu, J. Verhoeven, E. J. Puik, and M. J. van der Wiel, Appl. Surf. Sci. **78**, 147 (1994).

[4] R. Schlatmann, J. D. Shindler, and J. Verhoeven, Phys. Rev. B **51**, 5345 (1995).

[5] S. F. Edwards and D. R. Wilkinson, Proc. R. Soc. London A **381**, 17 (1982).

[6] H. Konig and G. Helwig, Optik **6**, 111 (1950).

[7] J. M. Bradley and J. M. E. Harper, J. Vac. Sci. Technol. A **6**, 2390 (1988).

[8] C. Herring, in *The Physics of Powder Metallurgy*, edited by W. E. Kingston (McGraw Hill, New York, 1951), pp. 143–179.

[9] W. W. Mullins, J. Appl. Phys. **30**, 77 (1959).

[10] K. Oyoshi, T. Tagami, and S. Tanaka, Jpn. J. Appl. Phys. **30**, 1854 (1991).

[11] C. Volkert and A. Polman, in *Phase Formation and Modification by Beam-Solid Interactions*, edited by G. S. Was, L. E. Rehn, and D. Follstaedt, Symposia Proceedings No. 235 (Materials Research Society, Pittsburgh, 1992), p. 3.

[12] D. G. Stearns, J. Appl. Phys. **71**, 4286 (1992).

[13] D. G. Stearns, Appl. Phys. Lett. **62**, 1745 (1993).

[14] E. Spiller, D. G. Stearns, and M. Krumrey, J. Appl. Phys. **74**, 107 (1993).

[15] M. Kardar, G. Parisi, and Y. C. Zhang, Phys. Rev. Lett. **56**, 889 (1986).

[16] T. M. Mayer, E. Chason, and A. J. Howard, J. Appl. Phys. **76**, 1633 (1994).

[17] For a general review, see J. Krug and H. Spohn, in *Solids Far From Equilibrium: Growth, Morphology and Defects*, edited by C. Godreche (Cambridge University Press, Cambridge, England, 1991).

[18] D. E. Savage, J. Kleiner, N. Schimke, Y. H. Phang, T. Janowski, J. Jacobs, R. Kariotis, and M. G. Lagally, J. Appl. Phys. **69**, 1 (1991).

[19] M. K. Sanyal, S. K. Sinha, and A. Gibaud, in *Interface Dynamics and Growth*, edited by K. S. Liang, M. P. Anderson, R. F. Bruinsma, and G. Scoles, MRS Symposia Proceedings No. 237 (Materials Research Society, Pittsburgh, 1992).

[20] E. Chason and T. M. Mayer, Appl. Phys. Lett. **62**, 363 (1993).

[21] E. Chason, T. M. Mayer, B. K. Kellerman, D. T. McIlroy, and A. J. Howard, Phys. Rev. Lett. **72**, 3040 (1994).

[22] E. A. Eklund, R. Bruinsma, J. Rudnick, and R. S. Williams, Phys. Rev. Lett. **67**, 1759 (1991).

[23] E. A. Eklund, E. J. Snyder, and R. S. Williams, Surf. Sci. **285**, 157 (1993).

[24] J. Krim, I. Heyvaert, C. van Haesendonck, and Y. Bruynseraede, Phys. Rev. Lett. **70**, 57 (1993).

[25] E. J. Puik, M. J. van der Wiel, H. Zeijlemaker, and J. Verhoeven, Rev. Sci. Instrum. **63**, 1415 (1992).

[26] E. Louis, H.-J. Voorma, N. B. Koster, L. Shmaenok, F. Bijkerk, Yu. Ya. Platonov, S. Yu. Zuev, S. S. Andreev, E. A. Shamov, and N. N. Salashchenko, Microelectron. Eng. **27**, 235 (1995).

[27] A. Kloidt, H. J. Stock, U. Kleineberg, T. Döring, M. Pröpper, B. Schmiedeskamp, and U. Heinzmann, Thin Solid Films **228**, 154 (1993).

[28] E. Spiller, J. Wilczyncski, L. Golub, and G. Nystrom, Proc. Soc. Photo-Opt. Instrum. Eng. **1546**, 168 (1991).

[29] S. K. Sinha, E. B. Sirota, S. Garoff, and H. B. Stanley, Phys. Rev. B **38**, 2297 (1988).

[30] For an overview of surface x-ray and neutron scattering, see *Surface X-ray and Neutron Scattering, Springer Series in Physics Vol. 61*, edited by H. Zabel and I. K. Robinson (Springer, Berlin, 1992).

[31] J. Als-Nielsen, F. Christensen, and P. S. Pershan, Phys. Rev. Lett. **48**, 1107 (1982).

[32] M. K. Sanyal, S. K. Sinha, K. G. Huang, and B. M. Ocko, Phys. Rev. Lett. **66**, 628 (1991).

[33] I. M. Tidswell, T. A. Rabedeau, P. S. Pershan, and S. D. Kosowsky, Phys. Rev. Lett. **66**, 2108 (1991).

[34] J. D. Shindler, E. A. L. Mol, A. Shalaginov, and W. H. de Jeu, Phys. Rev. Lett. **74**, 722 (1995).

[35] R. Schlatmann, Ph.D. thesis, Free University of Amsterdam, 1995.

[36] M. P. Bruijn, P. Chakraborty, H. W. van Essen, J. Verhoeven, and M. J. van der Wiel, Proc. SPIE **563**, 36 (1985).

[37] J. D. Shindler and R. M. Suter, Rev. Sci. Instrum. **63**, 5343 (1992).

[38] T. Salditt, T. H. Metzger, and J. Peisl, Phys. Rev. Lett. **73**, 2228 (1994).

[39] L. G. Parratt, Phys. Rev. **95**, 359 (1954).

[40] V. Holy, J. Kubena, I. Ohlidal, K. Lischka, and W. Plotz, Phys. Rev. B **47**, 15 896 (1993).

[41] J. B. Kortright, J. Appl. Phys. **70**, 3620 (1991).

[42] Y. H. Phang, D. E. Savage, R. Kariotis, and M. G. Lagally, J. Appl. Phys. **74**, 3181 (1993).

[43] A. Petford-Long, M. B. Stearns, C. H. Chang, D. G. Stearns, N. M. Ceglio, and A. M. Hawrylak, J. Appl. Phys. **61**, 1422 (1987).

[44] J. M. Slaughter, P. A. Kearney, D. W. Schulze, C. M. Falco, C. R. Hills, E. B. Saloman, and R. N. Watts, Proc. SPIE **1343**, 73 (1990).